Supporting Information

Coffee-Driven Green Activation of Cellulose and Its Use for All-Paper Flexible Supercapacitors

Donggue Lee,[†] Yoon-Gyo Cho,[‡] Hyun-Kon Song,[‡] Sang-Jin Chun,[§] Sang-Bum Park,[§] Don-Ha Choi,[§] Sun-Young Lee,[§] JongTae Yoo,[*†] and Sang-Young Lee[*†]*

†Department of Energy Engineering, School of Energy and Chemical Engineering, Ulsan National Institute of Science and Technology (UNIST), Ulsan 44919, Korea

‡Department of Chemical Engineering, School of Energy and Chemical Engineering, Ulsan National Institute of Science and Technology (UNIST), Ulsan 44919, Korea

§Department of Forest Products, Korea Forest Research Institute, Seoul 02455, Korea

Correspondence and requests for materials should be addressed to S.-Y. Lee[§] (email: nararawood@Korea.kr), J. Yoo[†] (email: jongtaeyoo@unist.ac.kr), and S.-Y. Lee[†] (email: syleek@unist.ac.kr)

Experimental Section:

Materials. Commercially available paper towel (here, Kimwipes®) was used as received. Espresso coffee beans (Star espresso, Coffeeroasters Inc.) were purchased and ground to powders. Single-walled carbon nanotubes (SWNTs) (TUBALL, C purity > 75 %, outer mean diameter ~ 1.8 ± 0.4 nm, length > 5 μm) and multi-walled carbon nanotubes (MWNTs) (Nanocyl, C purity > 95 %, average diameter ~ 9.5 nm, average length ~ 1.5 μm) were used. Sodium dodecylbenzenesulfonate (SDBS), polyvinyl alcohol (PVA) (molecular weight = 89,000 − 98,000 g mol^{-1}), and polytetrafluoroethylene (PTFE) (60 wt% dispersion in water) were purchased from Sigma-Aldrich. Potassium hydroxide (KOH) and polydimethylsiloxane (PDMS) (Sylgard 184, base/curing agent) were purchased from Daejung Chemical & Metals Co., Ltd. and Sewang Hitech Co., Ltd., respectively.

Structural/physicochemical characterizations of EK-ACs and paper supercapacitors. The concentration of K^+ ions in the espresso was quantitatively estimated using inductively coupled plasma optical emission spectrometry (ICP-OES, 700-ES (Varian)). The morphologies of the EK-ACs and paper towel-containing components were characterized by field emission scanning electron microscopy (FE-SEM, S-4800 (HITACHI)) and energy dispersive X-ray spectroscopy (EDS, JSM 6400 (JEOL)). The microporous structure of the EK-ACs was analyzed using high-resolution transmission electron microscopy (HRTEM, JEM-2100F (JEOL)) and X-ray photoelectron spectroscopy (XPS, K-Alpha™$^+$ XPS system (Thermo Scientific™)). The specific surface area of the EK-ACs was analyzed with N_2 adsorption-desorption isotherms at 77 K using physisorption analyzer ASAP2020 (Micromeritics). The pore size distribution of the EK-ACs was determined using the t-plot method applied to the adsorption branch of the isotherm. The graphitic carbons of the EK-

ACs were identified using X-ray diffraction (XRD, D8 Advance (Bruker)) measurements at 40 kV and 40 mA (CuK_α radiation, λ = 0.154056 nm). The thermogravimetric analysis (TGA) was conducted using an SDT Q600 (TA Instruments) in N_2 atmosphere (heating rate = 5 ˚C min^{-1}). The Fourier transform infrared (FT-IR), visible-near infrared (vis-NIR), and Raman spectroscopy measurements were performed using a Varian 660-IR (Varian Medical Systems, Inc.), Cary 5000 (Agilent), and Alpha300R (WITec), respectively. The water contact angle of the paper packaging substance was measured by a drop shape analyzer (DSA100, KRUSS). The porosity of paper towels was measured using mercury intrusion porosimetry (AutoPore IV 9500, Micromeritics Instrument Corp.). The electronic resistance of the electrode sheets was estimated using a FPP-RS8 (Dasoleng Corp., Korea) based on a dual-configuration four-point probe (FPP) technique. The particle size distribution of the EK-ACs was determined using a particle size analyzer (PSA 1090, CILAS).

Electrochemical/mechanical characterization of EK-ACs and paper supercapacitors. To investigate the electrochemical properties of the EK-ACs, an electrode paste (EK-ACs/MWNT/PTFE = 85/10/5 (w/w/w) was pressed into a nickel foam current collector using a roll press machine. A coin (2032-type) cell was fabricated by symmetrically assembling the as-prepared electrodes with a Celgard 3501 separator (thickness = 25 μm), with 6 M KOH aqueous solution injected as a liquid electrolyte. The cyclic voltammograms (CVs) and galvanostatic charge-discharge (GCD) profiles of the supercapacitor cells were determined using a potentiostat/galvanostat (VSP classic, Bio-Logic) at various scan rates in the potential range of 0.0 − 0.8 V. The electrochemical impedance spectroscopy (EIS) data for the cells were recorded at an applied voltage of 10 mV in the frequency range 10^{-3} to 10^5 Hz. The mechanical bending tests of the cells were carried out with a universal testing machine (DA-01, Petrol LAB) at a strain rate of 500 mm min^{-1}.

Transmission Line Model with Pore Size Distribution (TLM-PSD):

Total ionic conductance through pores can be calculated as follows:

$$Y_p = \kappa V_{tot} / l_p^2 \qquad (1)$$

Y_p: total ionic conductance through pores (Ω^{-1})

κ: electrolyte conductivity (Ω^{-1} cm^{-1})

V_{tot}: total pore volume (cm^3)

l_p: length of a pore (cm)

The penetrability is expressed as follows:

$$\alpha = \left(\frac{1}{2 l_p} \sqrt{\frac{\kappa r}{C_d}} \right) \omega^{-0.5} = \alpha_0 \omega^{-0.5}$$

α: penetrability (dimensionless)

α_0: penetrability coefficient

r: radius of a pore (cm)

C_d: electric double layer capacitance (F cm^{-2})

ω: angular frequency (rad s^{-1}).

Methodology for the TLM-PSD was not concretely commented in this article, for definition or formulation, see the nomenclature and references[1-3].

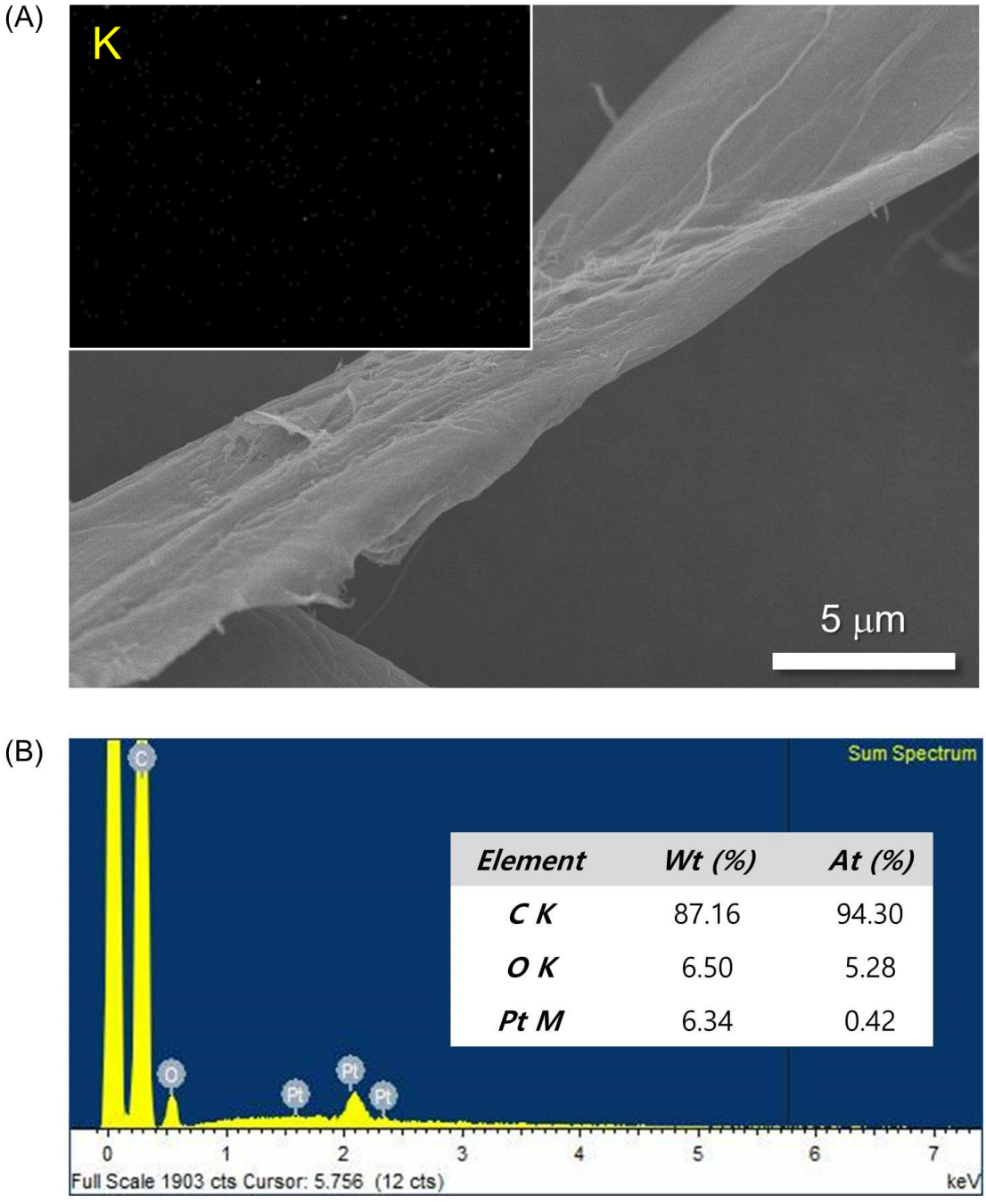

Figure S1. Structural characterization of the K-ACs. (A) SEM image and (inset) EDS mapping image (yellow dots represent elemental K). (B) EDS spectrum.

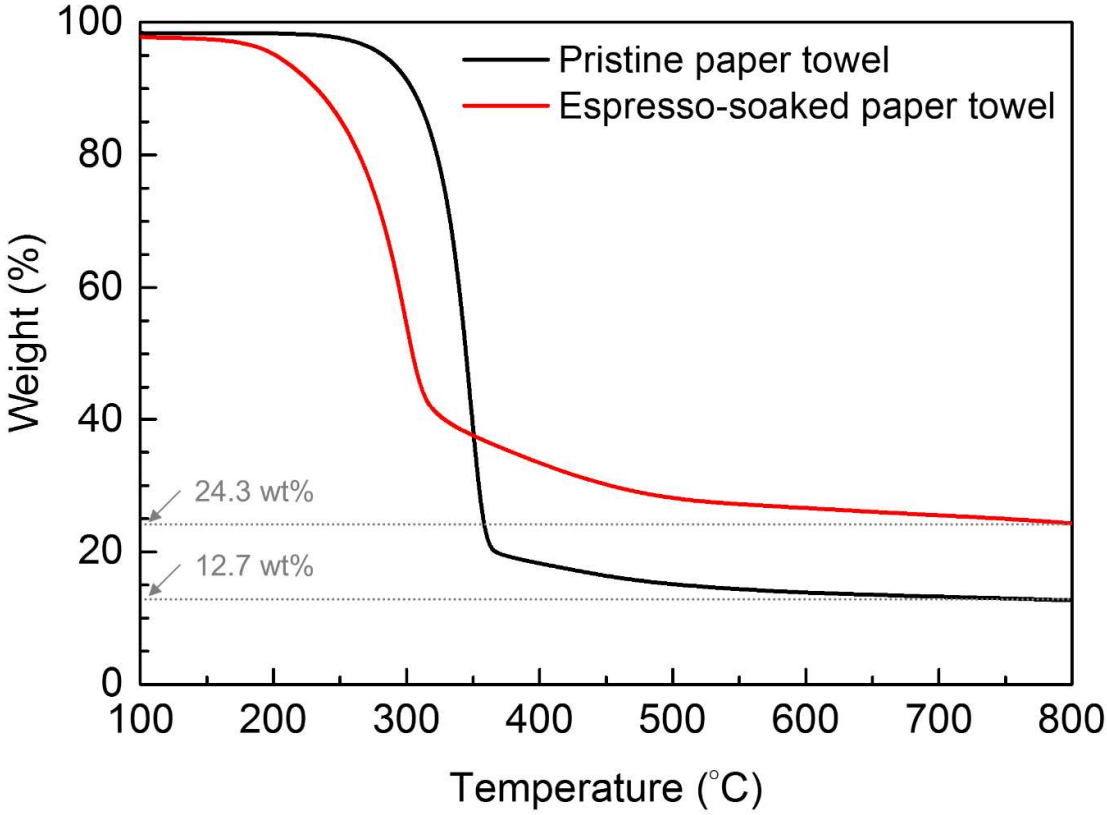

Figure S2. TGA profiles of the pristine (black line) and espresso-soaked (red line) paper towels.

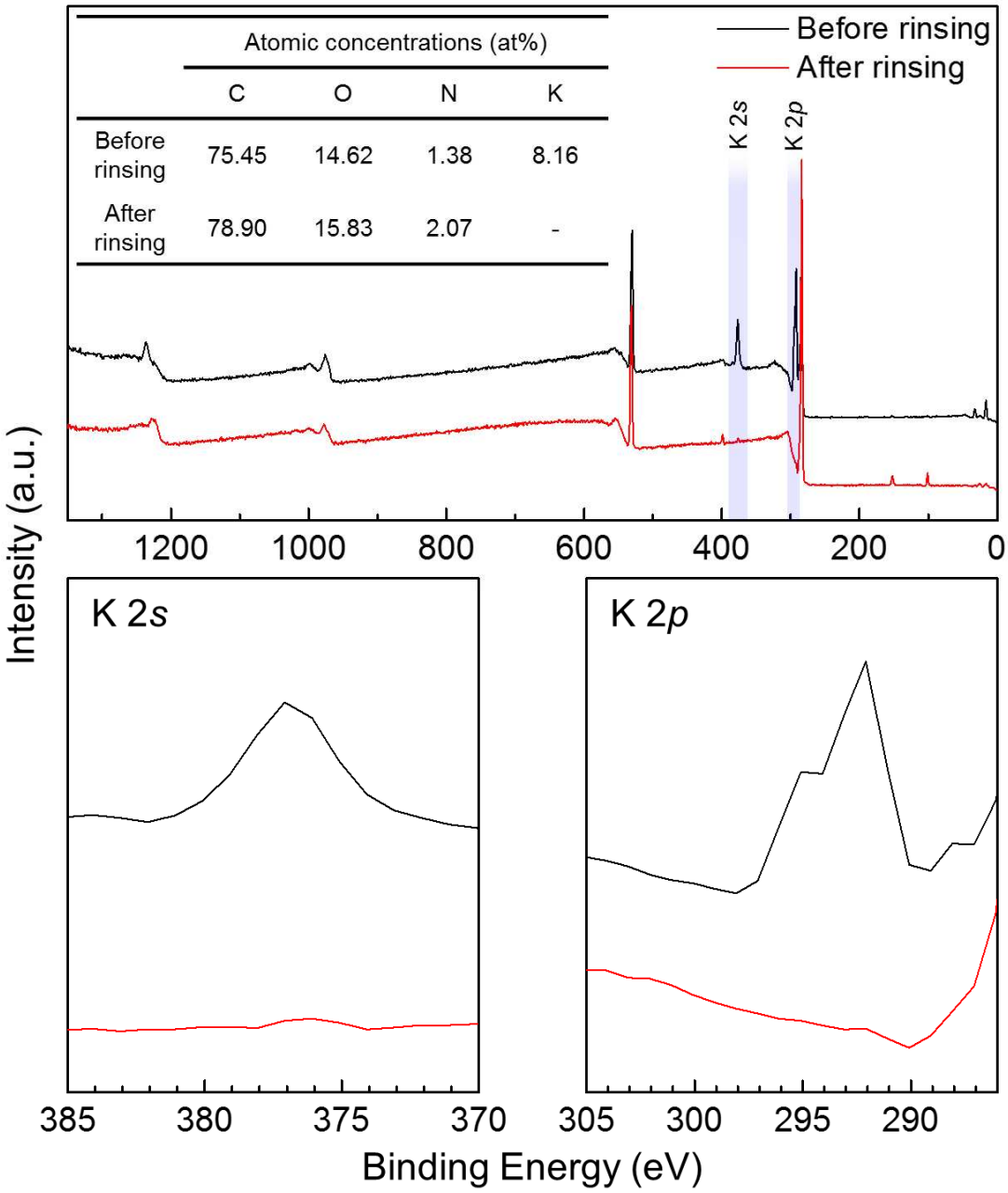

Figure S3. XPS spectra of the EK-AC before (black line) and after (red line) water rinsing, with a focus on K 2*s* and K 2*p* peaks. Atomic concentrations of the C, O, N, and K elements are presented in the inset table.

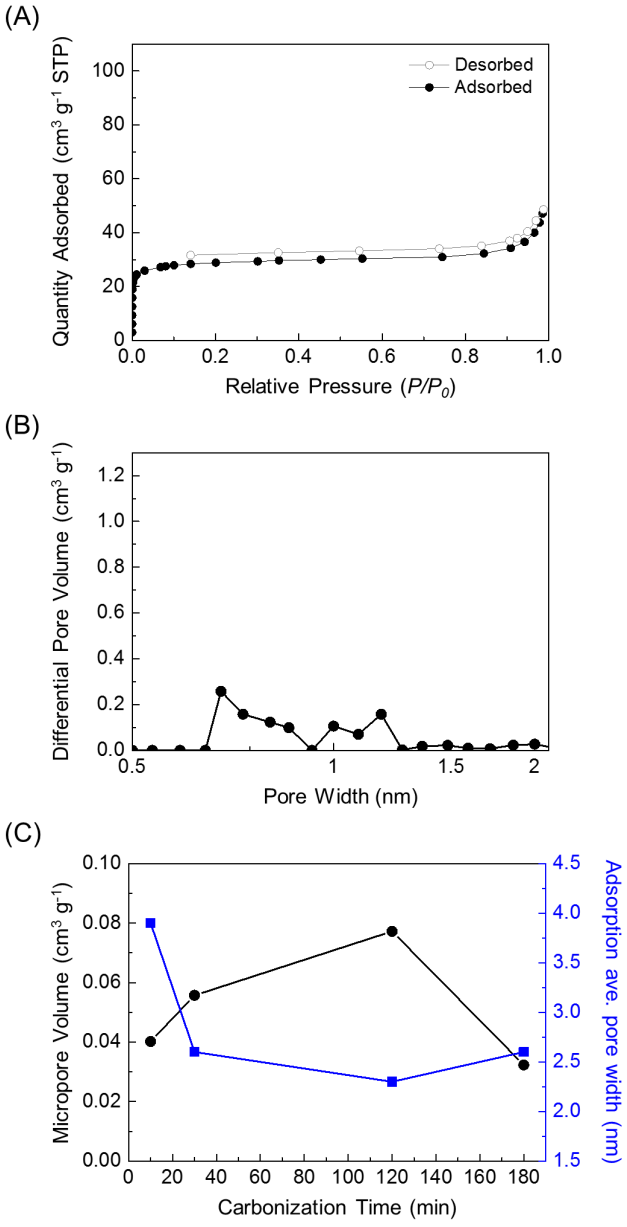

Figure S4. (A) N_2 adsorption-desorption isotherm and (B) pore size distribution of the EK-ACs (after water rinsing) carbonized for 180 min. (C) Comparison of micropore volume and adsorption average pore diameter of the EK-ACs (after water rinsing) as a function of carbonization time (10, 30, 120, and 180 min).

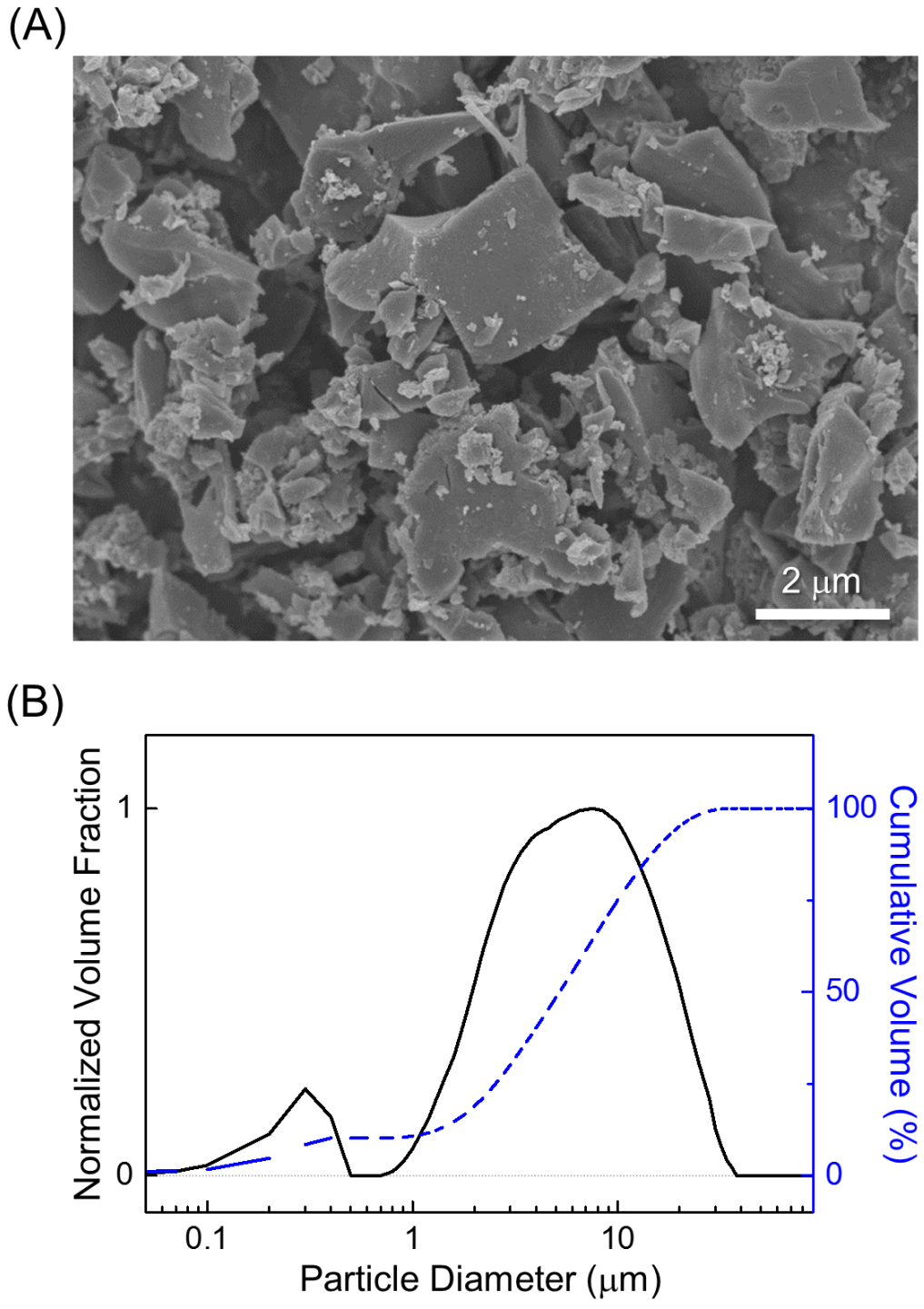

Figure S5. (A) SEM image and (B) particle size distribution of the EK-AC powders obtained by bead milling of the as-synthesized EK-ACs.

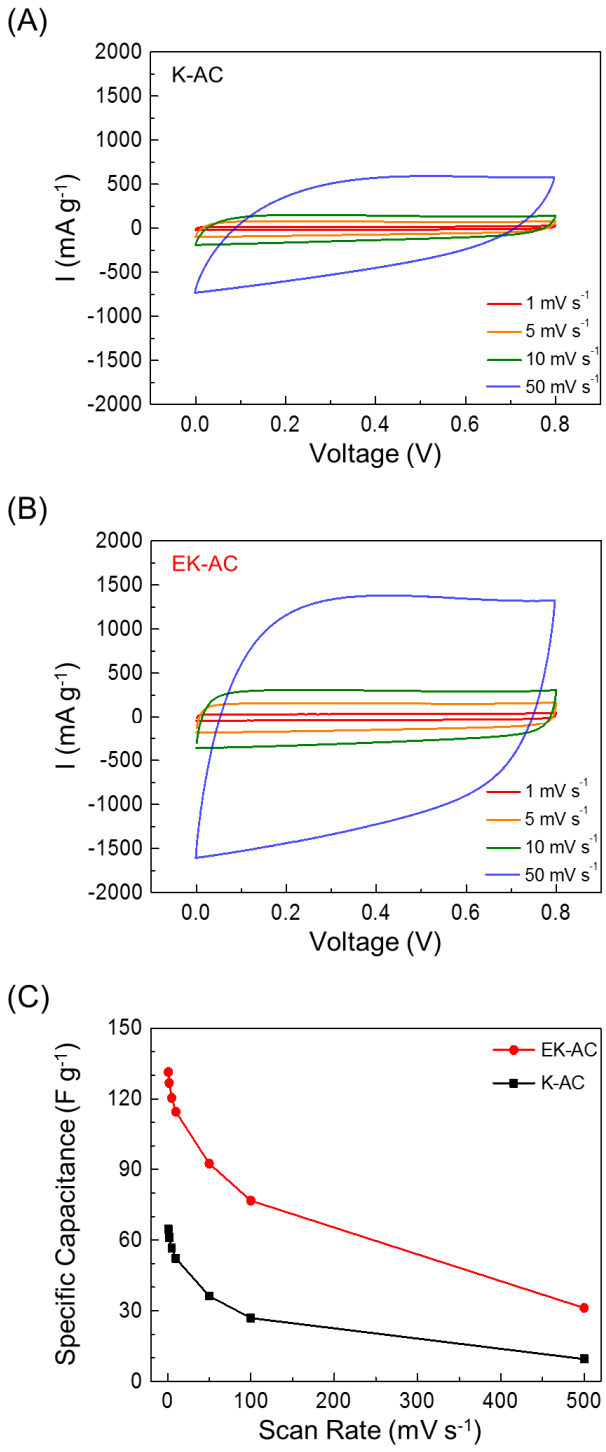

Figure S6. CV profiles (at scan rates = 1 − 50 mV s^{-1}) of the cells incorporating: (A) K-AC and (B) EK-AC. (C) Comparison in the specific capacitance between the EK-AC and K-AC as a function of the scan rate (= 1 – 500 mV s^{-1}).

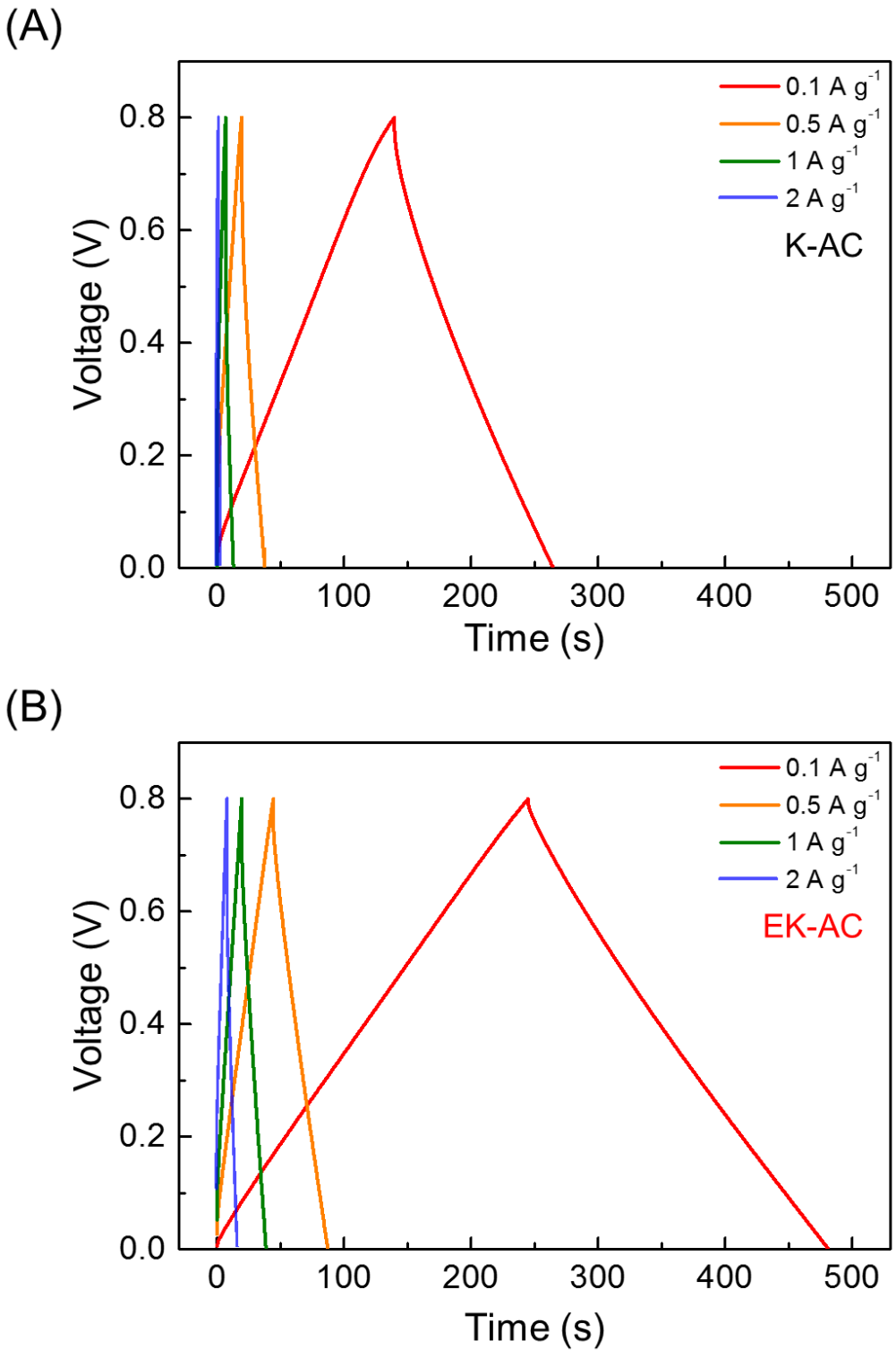

Figure S7. GCD profiles (at current densities = 0.1 – 2.0 A g^{-1}) of the cells incorporating: (A) K-AC and (B) EK-AC.

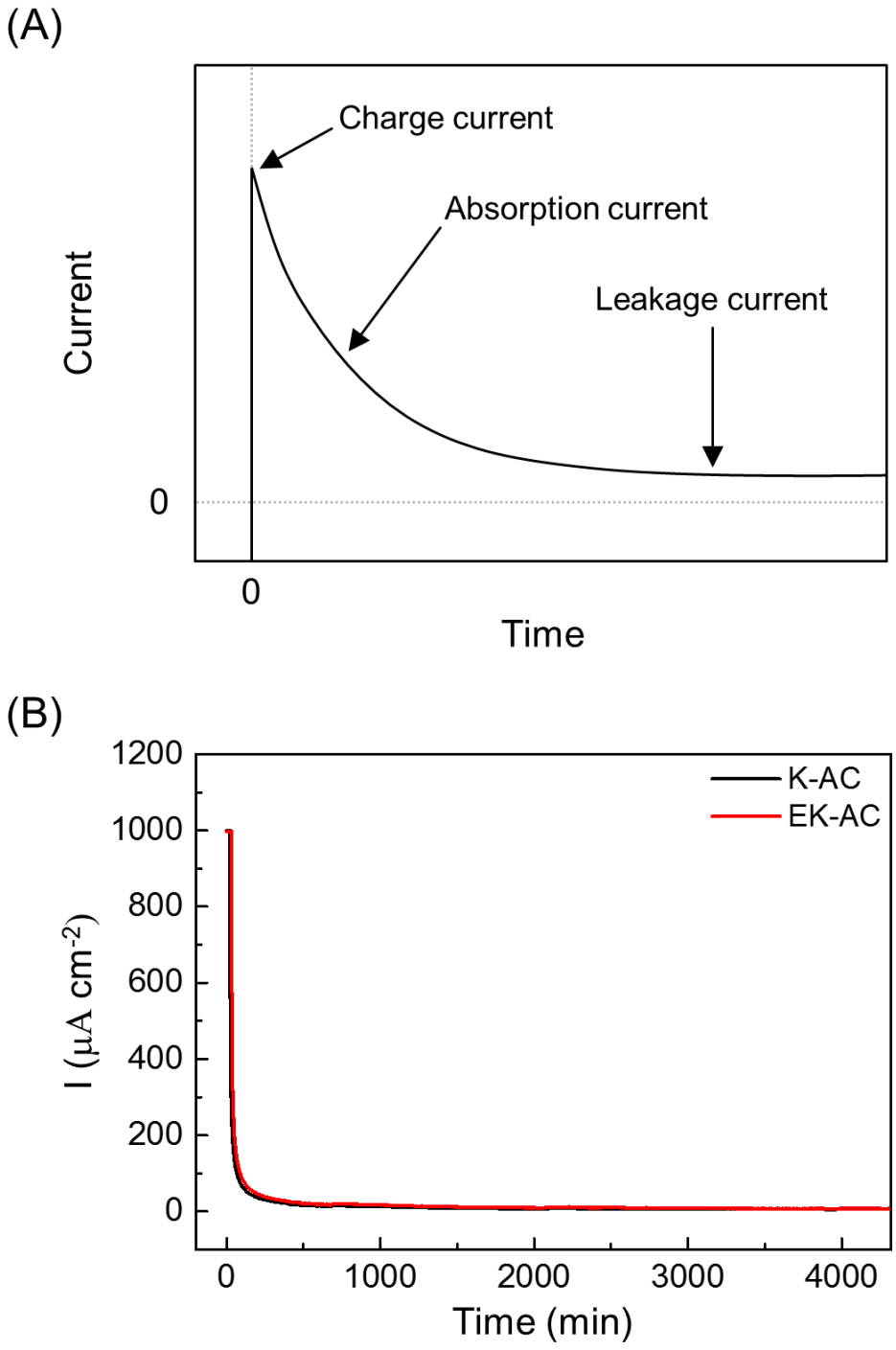

Figure S8. (A) A schematic image representing the charge, absorption, and leakage currents recorded under a constant voltage. (B) Comparison in the leakage current curves (at a constant voltage of 0.8 V) of SC cells assembled with the K-AC and EK-AC electrodes.

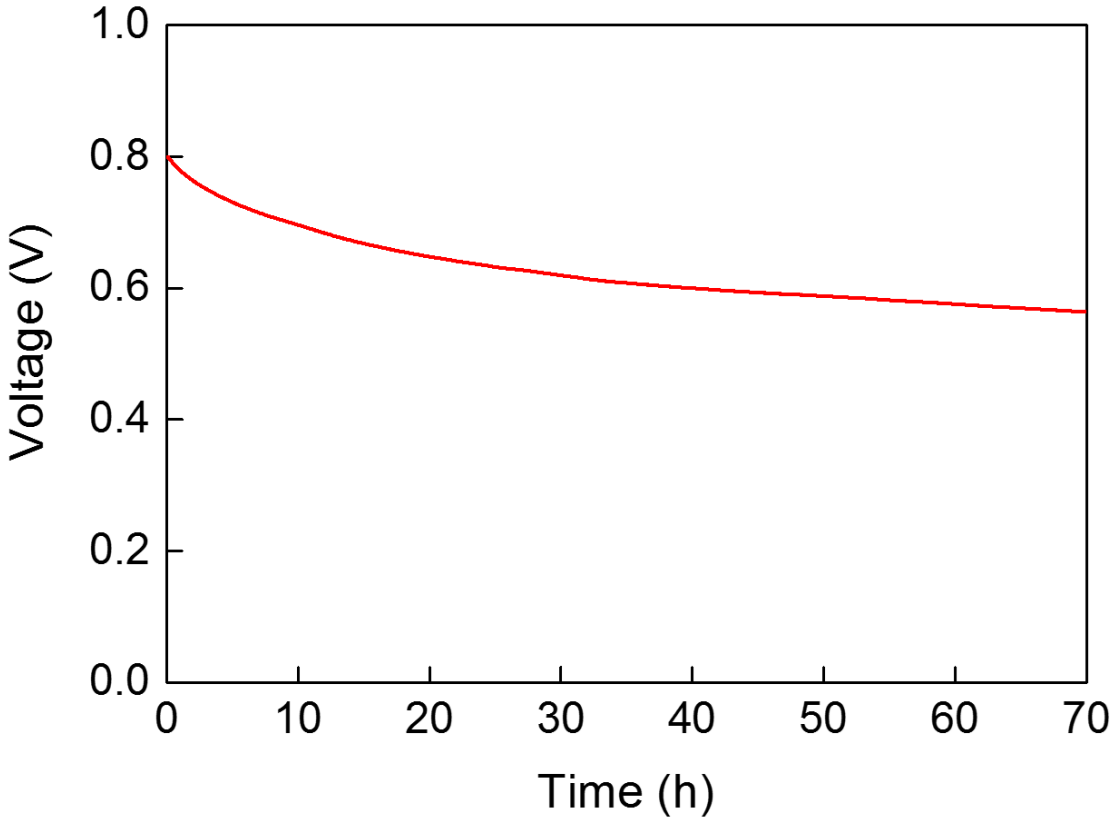

Figure S9. OCV profile of the cell containing the EK-AC. The cell was charged to 0.8 V at a constant current of 1 mA cm^{-2} and its OCV drop was monitored as a function of elapsed time.

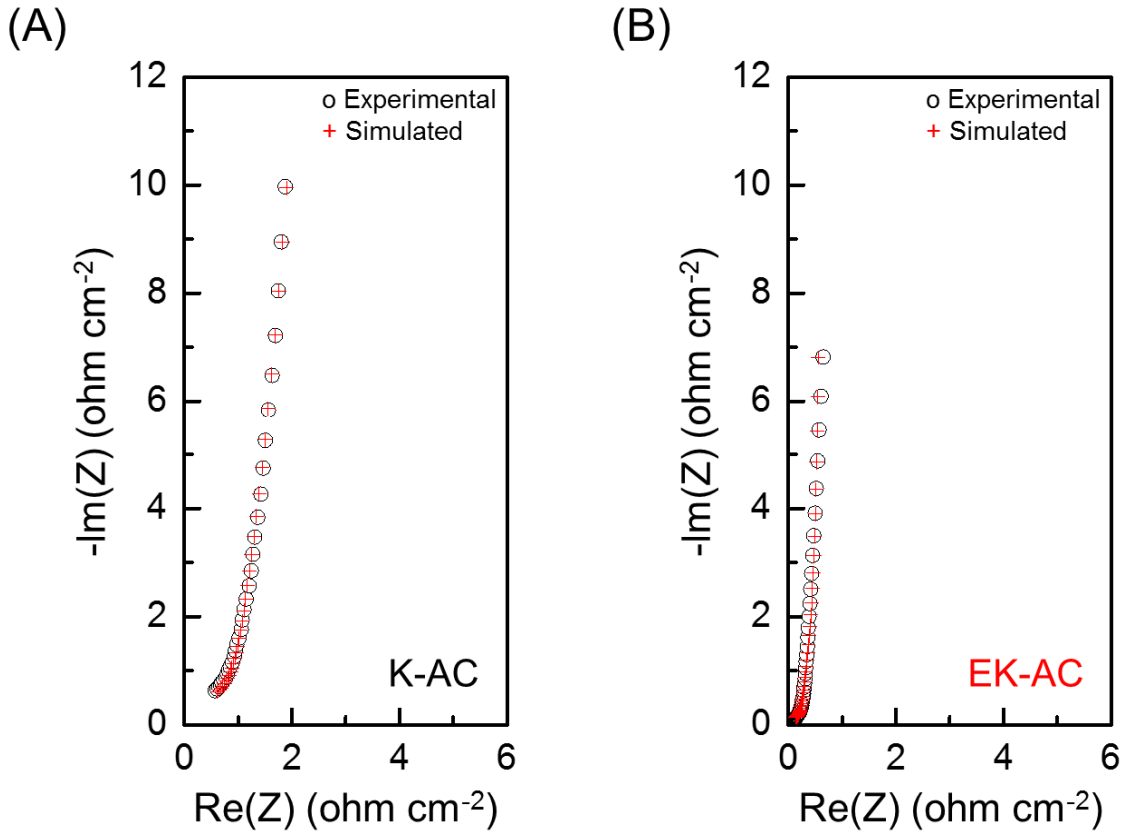

Figure S10. Impedance spectra of the cells incorporating: (A) K-AC and (B) EK-AC, in which black circles and red cross represent experimental and simulation results (calculated from the TLM-PSD model), respectively.

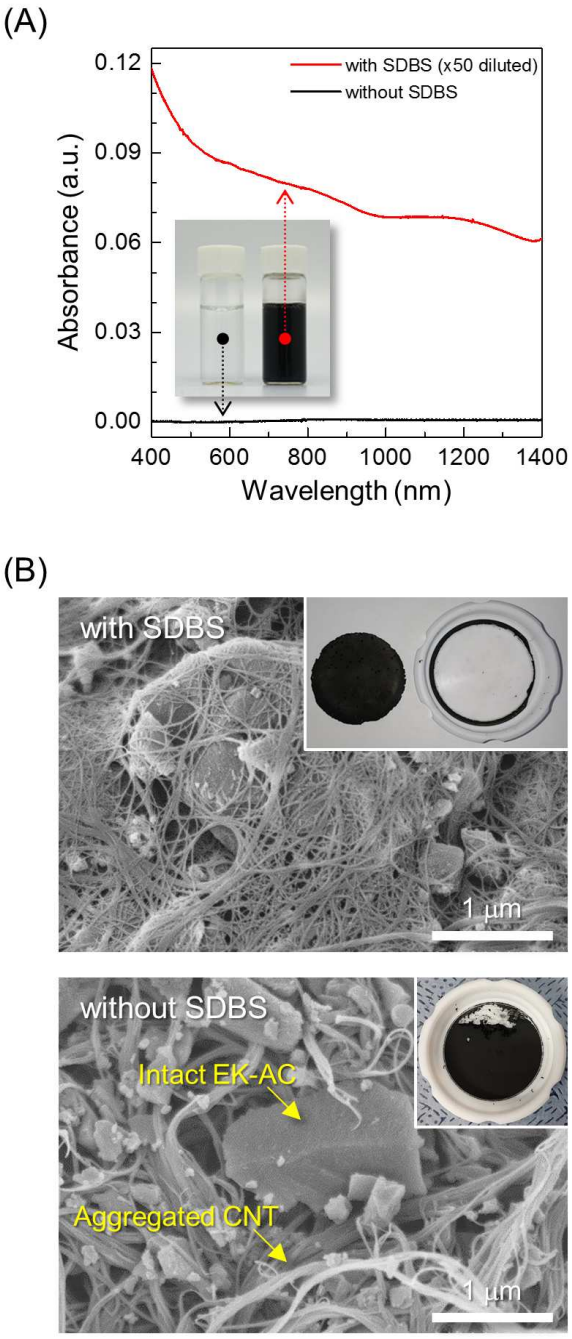

Figure S11. (A) Vis-NIR spectra and (inset) photographs of the SWNT suspensions, in which the SWNT suspensions were subjected to centrifugation (10,000 × *g*) and then the top layers (*i.e.*, supernatants) of the centrifuged suspensions were exclusively collected for this measurement. (B) SEM images of the EK-AC/SWNT composites: (top) with SDBS and (bottom) without SDBS. Insets show the physical appearance of the as-prepared EK-AC/SWNT composites.

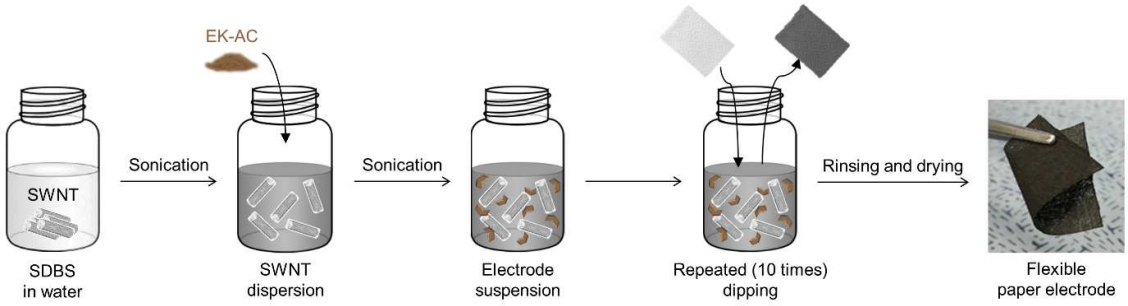

Figure S12. Schematic representation depicting the fabrication procedure and photograph of the EK-AC/SWNT-embedded paper electrode.

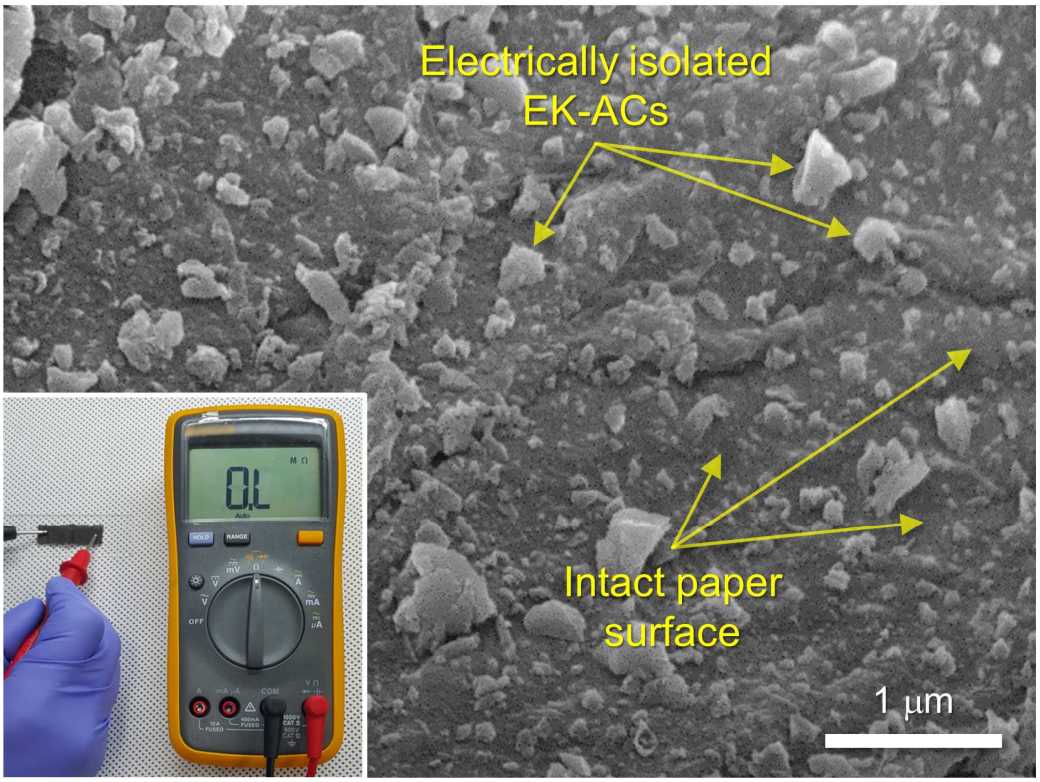

Figure S13. SEM image of the control paper electrode (containing EK-ACs without SWNTs), wherein the inset shows its surface electrical resistance.

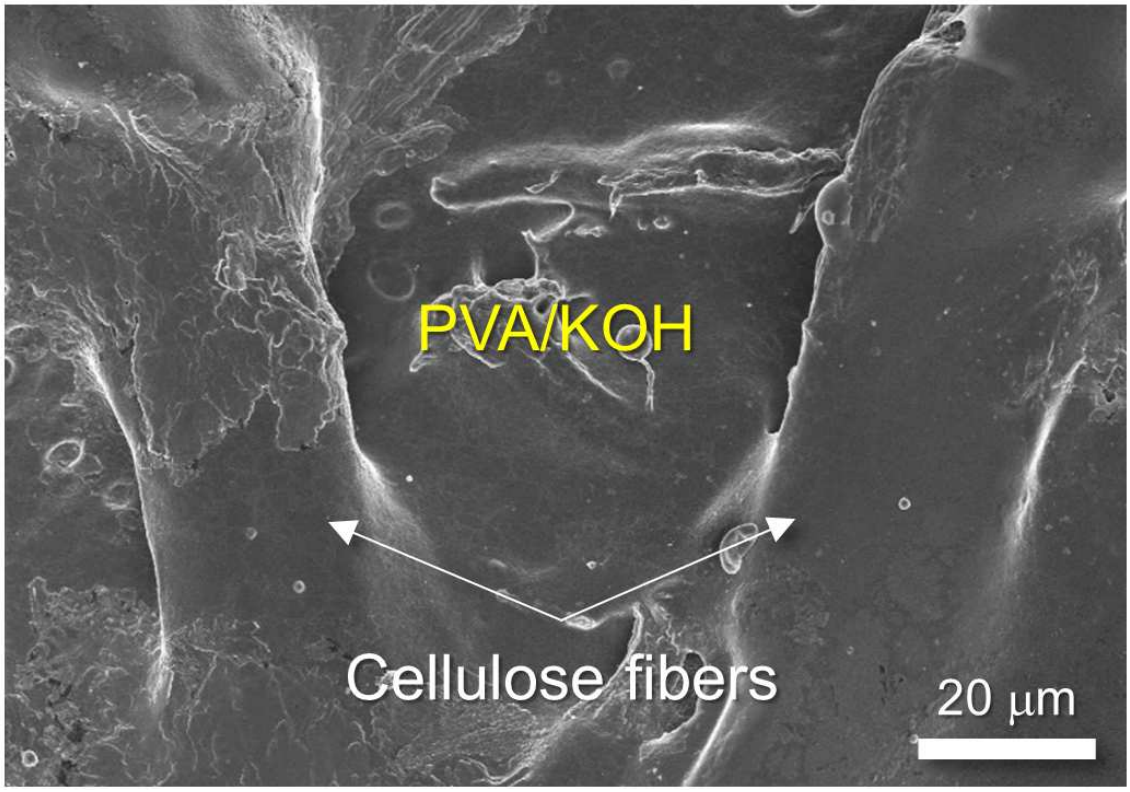

Figure S14. SEM image of the paper towel-reinforced PVA/KOH composite polymer electrolyte.

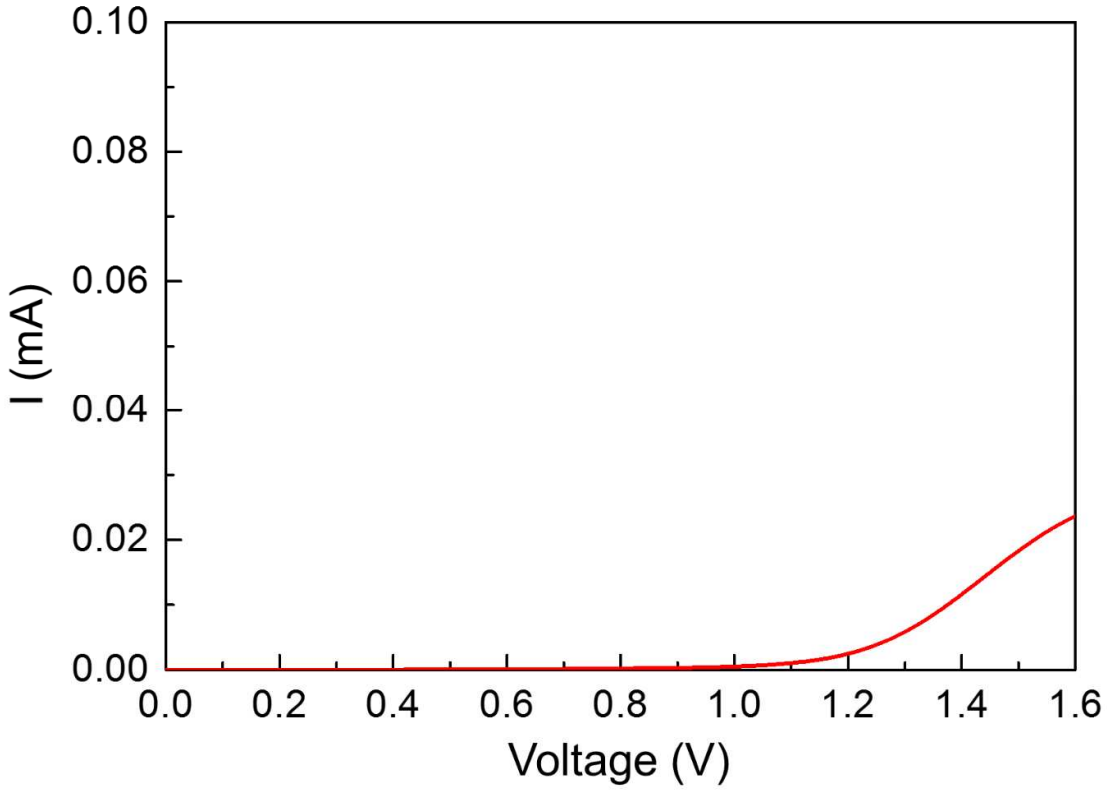

Figure S15. LSV profile of the paper towel-reinforced PVA/KOH composite polymer electrolyte (at scan rate = 1 mV s^{-1}).

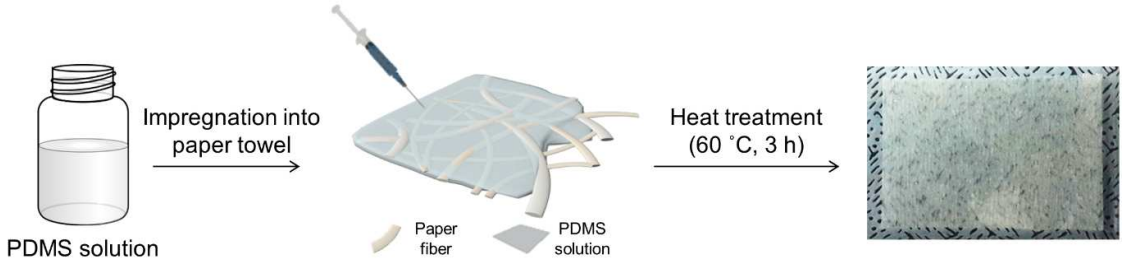

Figure S16. Schematic representation depicting the fabrication procedure and photograph of the PDMS-infiltrated paper towel as a packaging substance.

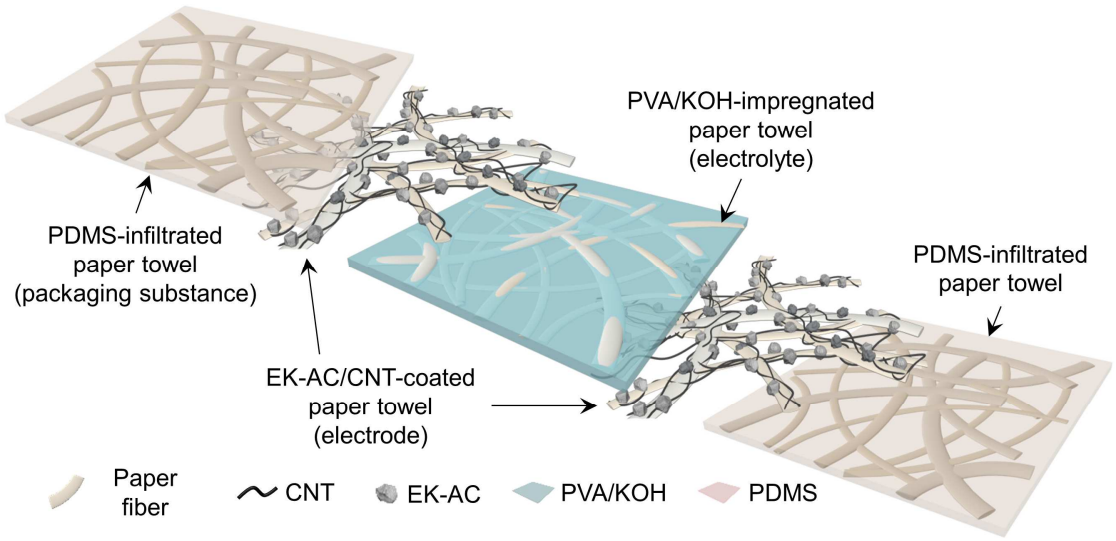

Figure S17. Schematic illustration depicting the structure of the all-paper flexible electric double-layer supercapacitor.

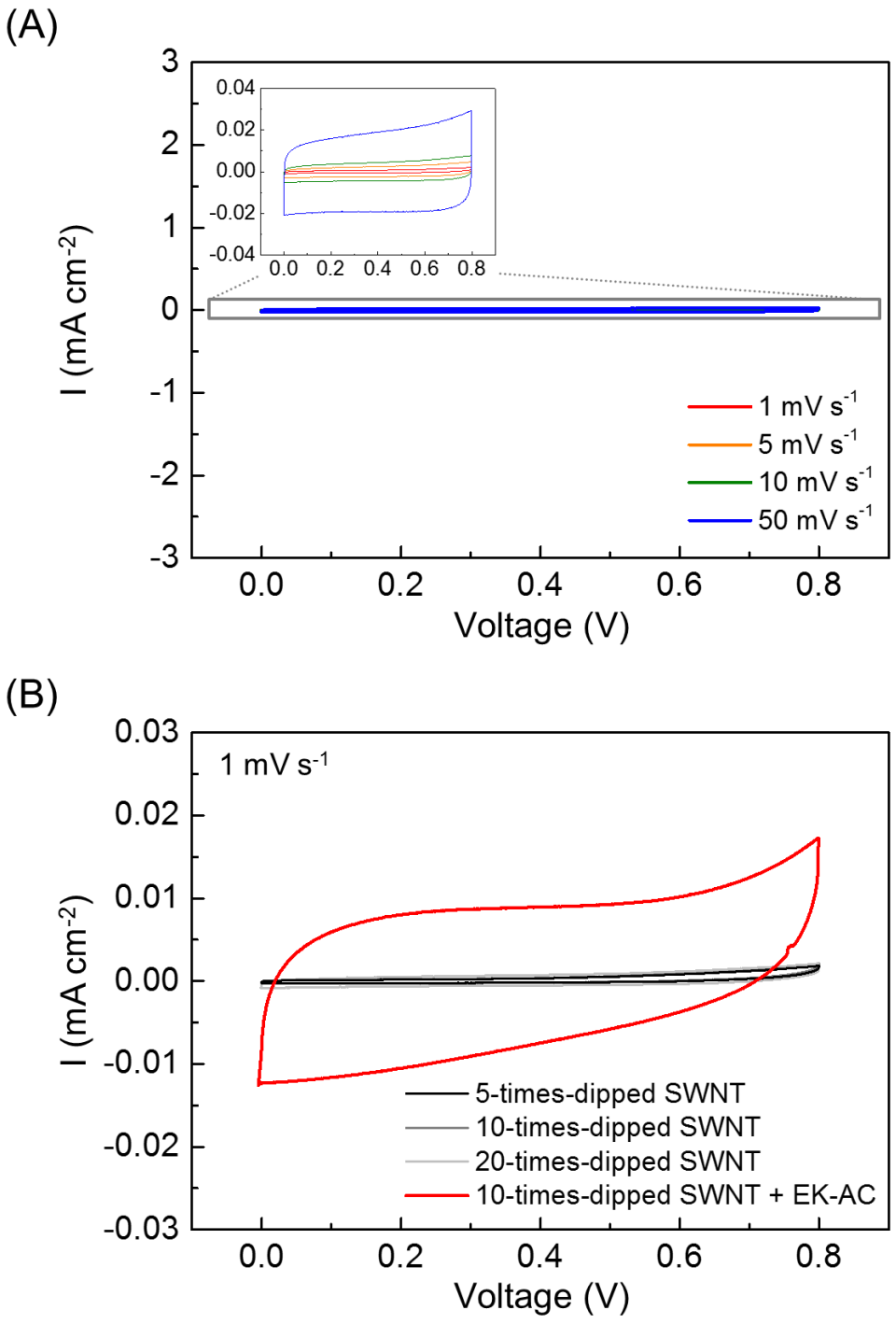

Figure S18. (A) CV profiles of control paper electrodes (containing SWNTs without EK-ACs) measured at scan rates of 1 − 50 mV s^{-1}. (B) Comparison of CV profiles between the control paper electrodes (prepared as a function of dipping number) and the EK-AC paper electrode (containing SWNTs and EK-ACs).

Table S1. Comparison of the specific surface area (SSA), capacity, SSA increment (per moles of K^+ ions), and capacity increment (per moles of K^+ ions) for K-AC, EK-AC and KOH activation (chosen as a control sample)-based AC.

	K-AC	**EK-AC**	**Control**
Moles of K^+ ions (mmol g_{paper}^{-1})	-	1.075	4.349
SSA ($m^2\ g^{-1}$)	198.89	255.80	609.49
Capacity ($F\ g^{-1}$)	64	131	219
SSA increment per moles of K^+ ions ($m^2\ mol^{-1}$)	-	52.94×10^3	94.41×10^3
Capacity increment per moles of K^+ ions ($F\ mol^{-1}$)	-	62.33×10^3	35.64×10^3

Table S2. Comparison in electrochemical performance of biomass-derived electrode materials for supercapacitors (This work vs. Previous studies).

Publication	Biomass used for synthesizing ACs	Activation agent	Electrolyte	Capacitance of ACs	Cycling performance
This study	**Commercial paper towel**	**Coffee**	**6 M KOH**	**131 F g^{-1} (1 mV s^{-1})**	**100 % after 10000 cycles**
			PVA/KOH	**103.5 mF cm^{-2} (1 mV s^{-1})**	**89 % after 5000 cycles**
Nat. Commun. **2016**, *7*, 11586.	Cotton textile	1 M NaF solution	6 M KOH	90.1 F g^{-1} (2.5 A g^{-1})	-
Nano Energy **2016**, *25*, 161–169.	Cellulose nanofibril	-	Ionic liquid ([BMPy][TFSI])	84 F g^{-1} (0.1 A g^{-1})	92 % after 10000 cycles
ACS Appl. Mater. Interfaces **2016**, *8*, 3175−3181.	Citrus peel	KOH solution	1 M $NaClO_4$	110 F g^{-1} (0.1 A g^{-1})	64 % after 100000 cycles
RSC Adv. **2015**, *5*, 15438–15447.	Cotton textile	1 M NaF solution	6 M KOH	120 F g^{-1} (5 mV s^{-1})	-
J. Power Sources **2015**, *294*, 150–158.	Carbon fiber cloth	-	0.1 M Na_2SO_4	0.78 F g^{-1} (0.1 A g^{-1})	100 % after 10000 cycles
ACS Nano **2013**, *7,* 5131–5141.	Hemp bast fiber	KOH powder	Ionic liquid ([BMPy][TFSI])	110−144 F g^{-1}	96 % after 10000 cycles
Adv. Mater. **2012**, *24*, 3246–3252.	Cotton T-shirt	1 M NaF solution	1 M Na_2SO_4	70.2 F g^{-1} (2 mV s^{-1})	-

Table S3. Comparison of electrochemical performance for flexible supercapacitors (This work vs. Previous studies).

Publication	Type of active materials	Electrolyte	Capacitance	Cycling performance
This study	**Carbonized paper**	**6 M KOH**	**131 F g^{-1} (1 mV s^{-1})**	**100 % after 10000 cycles**
		PVA/KOH	**103.5 mF cm^{-2} (1 mV s^{-1})**	**89 % after 5000 cycles**
Adv. Energy Mater. **2017**, *7*, 1601847.	MXene/graphene	PVA/H_3PO_4	3.26 mF cm^{-2} (2 mV s^{-1})	85.2 % after 2500 cycles
ACS Nano **2016**, *10*, 11351−11359.	Activated carbon	1 M H_2SO_4	63.2 F g^{-1} (0.1 A g^{-1})	100 % after 10000 cycles
Energy Environ. Sci. **2016**, *9*, 2812−2821.	Activated carbon	[BMIM][BF_4]/ETPTA	100 mF cm^{-2} (0.2 mA cm^{-2})	~ 99 % after 10000 cycles
Nano Energy **2015**, *13*, 306–317.	$NiCo_2O_4$/graphene paper	PVA/LiOH	71.32 F g^{-1}	96.8 % after 5000 cycles
ACS Nano **2012**, *6*, 4020−4028.	Chemically modified graphene	1 M Na_2SO_4	93 F g^{-1} (1 A g^{-1})	-
Energy Environ. Sci. **2011**, *4*, 3368−3373.	graphite	1 M H_2SO_4	12 F g^{-1} (200 mA g^{-1})	90 % after 15000 cycles
Adv. Energy. Mater. **2011**, *1*, 917−922.	Graphene	PVA/H_2SO_4	120 F g^{-1} (1 mV s^{-1})	99.1 % after 5000 cycles

Movie S1. Video clip showing the mechanical flexibility of the paper supercapacitor.

REFERENCES

(1) Song, H.-K.; Jung, Y.-H.; Lee, K.-H.; Dao, L. H., Electrochemical Impedance Spectroscopy of Porous Electrodes: The Effect of Pore Size Distribution. *Electrochim. Acta* **1999,** *44*, 3513-3519.
(2) Song, H.-K.; Hwang, H.-Y.; Lee, K.-H.; Dao, L. H., The Effect of Pore Size Distribution on the Frequency Dispersion of Porous Electrodes. *Electrochim. Acta* **2000,** *45*, 2241-2257.
(3) Song, H.-K.; Sung, J.-H.; Jung, Y.-H.; Lee, K.-H.; Dao, L. H.; Kim, M.-H.; Kim, H.-N., Electrochemical Porosimetry. *J. Electrochem. Soc.* **2004,** *151*, E102-E109.